GEOPHYSICAL RESEARCH LETTERS, VOL. 28, NO. 3, PAGES 527-530, FEBRUARY 1, 2001

UARS MLS Observations of Gravity Waves Associated with the Arctic Winter Stratospheric Vortex

Jonathan H. Jiang and Dong L. Wu

Jet Propulsion Laboratory, California Institute of Technology, Pasadena, California

Abstract. Passive satellite microwave limb radiances were used to study interactions between gravity waves and stratospheric winds in mid- to high latitude winter. We found that the radiance variances depend significantly on the instrument line-of-sight (LOS) and the background wind. The radiance variances are outstanding at two viewing angles where the LOS is about 30^o or 90^o from the wind vector. Waves propagating in preferred directions likely cause the two optimal angles observed. The variances at the 90^o angle, located inside the polar vortex, seem produced by the gravity waves propagating nearly parallel to the wind direction. The variances at the 30^o angle, located near the edge of the vortex, are likely associated with perturbations propagating almost perpendicularly to the wind direction. The variance of both modes increases with the background wind speed, but saturation is observed for the waves inside the vortex as wind speed exceeds about *60m/s*. Interestingly, we also found that the temperature co-located with the variance inside the vortex is warmer by *20K* at background wind speeds *>60m/s*, which might be correlated with the wave breaking in the vortex.

1. Introduction

Atmospheric gravity waves often induce air temperature fluctuations which can be detected by satellite sensors [e.g. *Fetzer and Gille*, 1994, *Wu and Waters*, 1996a,b, and *Preusse et al.*, 2000]. The Upper Atmosphere Research Satellite Microwave Limb Sounder (UARS MLS) radiance variance data used for gravity wave studies are particularly sensitive to waves of long (*≥10km*) vertical and short (*~100km*) horizontal wavelengths. *Wu and Waters* [1996a,b] demonstrated that some distinct spatial and seasonal patterns in MLS radiance variance climatology may be linked to strong gravity wave activities at high latitudes of winter hemispheres and at sub-tropical summer hemispheres. The amplitudes of the MLS radiance variances increase with altitude at exponential rate ($e^{z/H}$) between *28* to *50km*, and nearly saturated at altitudes above that. *Wu and Waters* [1997] further discussed the ascending or descending orbital differences of the MLS data, which was thought due to the different viewing directions associated. They showed that some of the differences associated with ascending or descending orbits are reconciled with the notion that they are produced by vertical propagating gravity waves with the phase (or wave vector) moving downward and in opposite direction of the background wind velocity. Using a ray-tracing model, *Alexander* [1998] showed that the background winds could play an important role in determining the amplitude and spatial variations of the gravity wave variances observed by MLS. Regions with strong winds are where gravity waves are most observable. It was also argued that the near-zero growth of the MLS radiance variance data at high altitude showed by in *Wu and Waters* [1996b] could be explained in part by the Doppler shifting effect of the background winds. In the Doppler shifting theory, waves may not actually break but instead move out of MLS filter (waves with vertical wavelength *>10km*). Recent studies using the MLS data [e.g. *McLandress et al.*, 2000] have shown that the sensitivity of radiance variance to air temperature perturbation depends upon orientation of the instrument's line-of-sight (LOS) and measurement schemes used. Such dependence can yield useful information about wave generation, propagation, variation, and breaking mechanisms. Since the MLS saturated radiances corresponds to air temperatures well above the tropospheric wave source regions, the gravity waves observed in the stratosphere have undergone through the filtering by the background winds. Therefore, further analyzing the information of background wind would provide valuable insights on the interactions between gravity waves and jet streams in the stratosphere.

In this paper, we investigate viewing angle dependence of MLS radiance variance and its relationship to stratospheric background winds. We focus our analysis on the wave activities associated with Arctic winter (DJF) stratospheric vortex, using the background stratospheric winds from the global assimilation by the United Kingdom Meteorological Office (UKMO). During the winter season, although the stratospheric jet-stream travels mostly eastward, the actual path of the jet dips and rises at seemingly random places. This provides the MLS sampling with the ample amount of different angles between its LOS and the wind vectors which makes variance-wind relation study feasible.

2. Viewing angles θ_w, θ_k and the variance response function

In reality, we do not know the wave propagation direction but we know the angle between the MLS LOS and the UKMO horizontal wind velocity **U**. We here define θ_w as the angle with respect to the wind. On the other hand, *Wu and Waters* [1997] have simulated MLS filter response temperature fluctuations, which depends on the angle between the LOS and wave propagation direction. We call this angle θ_k, meaning the angle relative to the wave vector **k**.

Because MLS has a "cigar-shaped" temperature weighting function [*Wu and Waters*, 1996b, 1997], the radiance variances are sensitive to viewing angle θ_k. Figure 1, shows the simulated response of MLS variance as a function of θ_k for limb-tracking observation. The simulation has reflected

Paper number 2000GL011800.
0094-8276/01/2000GL011800$05.00

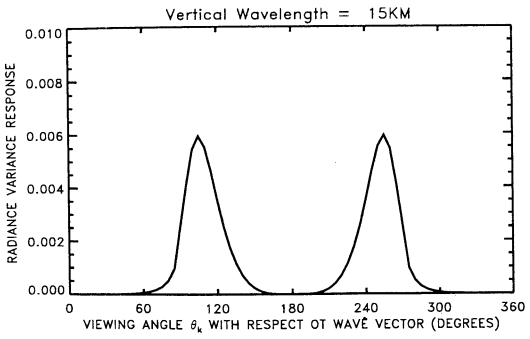

Figure 1. Simulated MLS limb-tracking variances response as a function of viewing angle for a vertical wavelength of 15km.

the integration over all horizontal wavelengths. According to this simulated variance response, the optimal θ_k angles are at about $\pm 110^o$ (i.e. about $\pm 20^o$ between the LOS and wave-front) for vertical wavelength λ_z=*15km*. In other words, the radiance variance is larger if the LOS direction is aligned close to (but not completely parallel to) the wave fronts. The reason that the optimal angle is slightly away from $\pm 90^o$ is due to the fact that the weighting function is titled with respect to a local observer. Thus, the response function is result of spatial filtering in the directions both along and cross the LOS. The optimal angles vary only slightly with λ_z.

In the following section, we will bin MLS radiance variances according to the background wind to obtain the θ_w-dependence. Knowing the LOS direction with respect to wind vector and the simulated θ_k-dependent response function, we hope to infer the orientation of the wave-front with respect to the wind vector.

The data we use in this study are the MLS limb-tracking radiance variances described by *Wu and Waters* [1996b]. We choose limb-tracking data other than the limb-scan data [*Wu and Waters*, 1996a] because the θ_k-dependent response function is much simpler to interpret in limb-tracking case. Thus, it is easier to further infer wave propagation properties.

3. Radiance variance observations in the jet-streams

On the north-looking orbits, MLS takes measurements over an area that covers the latitudes from *34°S* to *80°N*. The Arctic winter stratospheric jet-stream stretches from the pole to mid-latitudes allowing the observations made within strong wind fields. The observed data contain saturated radiances at eight different altitude layers of *28, 33, 38, 43, 48, 53, 61,* and *80km* [*Wu and Waters*, 1996b, 1997]. The variances of these radiances, which mimic the air temperature fluctuations at each layer, have been found to vary significantly with the angle between LOS direction and wind vectors.

In order to study the behavior of MLS variances inside the jet-stream, we first investigate the relation between the radiance variances and the angle θ_w (defined in the last section) at mid- to high latitudes (*45°N-80°N*). In Figure 2a, we illustrate the 1994-1997 wintertime (DJF) average radiance variances associated with wind speed *>10m/s*, as sorted by θ_w in *10°*-viewing-angle-bins from *0°* to *180°*. Each bin contains more than *1000* variance samples and the standard deviation of the samples varies from *10%-15%*, mostly due to atmospheric variability. Since the jet-stream mainly flows eastward in the winter season, measurements taken on the north-looking orbits fall mostly into the *0°-180°* viewing angles with respect to winds and very few samples (*<100*) are available in the *180°-360°* range, and thus the later range are not considered here.

In Figure 2a, there exist two modes that are significant in the θ_w-dependence of the variances. One variance mode peaks at θ_w~*90°* and dominates the variances at all the altitudes below *~48km*. This variance mode increases with altitude at exponential rate up to *~53km*, but show a smaller growth rate above that. Another variance mode takes maximum at θ_w~*30°*, grows with altitude continually, and gradually dominates variances at altitudes *≥53km*.

Based on the θ_k-dependent variance simulation (Figure 1), one may infer that the wave-front corresponding to the θ_w~*90°* variance mode should be nearly perpendicular to the wind direction, i.e. the wave vector points either to the direction of the wind or the opposite direction of the wind (see Figure 2b). For the θ_w~*30°* mode, the variance implies that the wave-front are almost parallel to the wind direction (see Figure 2c). However, given the θ_w-dependent and θ_k-dependent variance distributions, we could not determine which direction the waves are propagating: polar-ward or equator-ward.

We also investigate the dependence of variances on the background wind speed. Figure 3a,b show the radiance

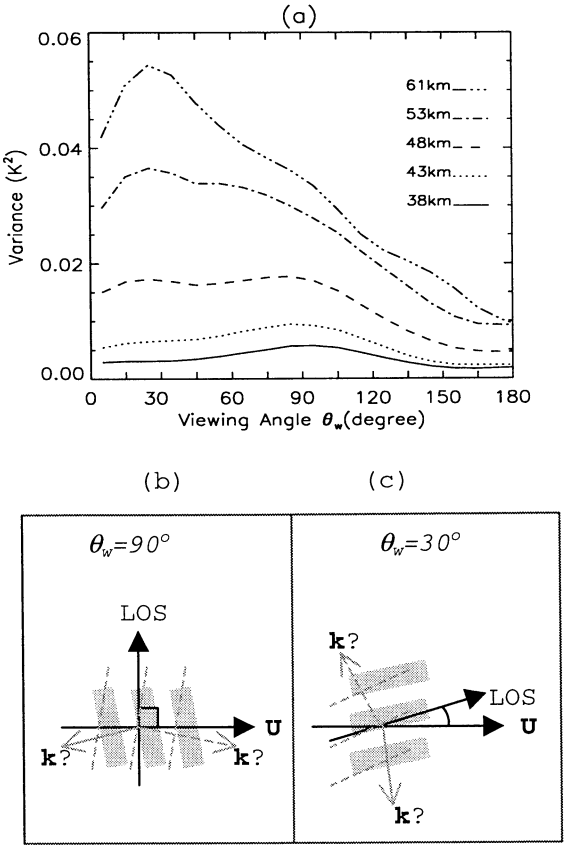

Figure 2. (a) Radiance variances observed by MLS as sorted by viewing angles θ_w defined in the text. (b) and (c) are schematic diagrams illustrate the horizontal direction of UKMO wind, LOS, and wave vector **k** for the θ_w=*90°* and θ_w=*30°* cases, respectively. The shaded boxes and dashed lines are footprints of wave fronts.

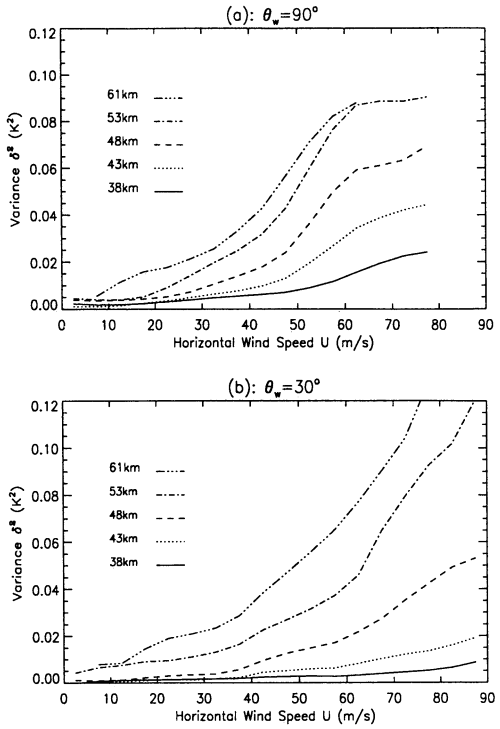

Figure 3. Radiance variances near θ_w=90° (a), and θ_w=30° (b) viewing angles sorted into different horizontal wind speeds.

variances at θ_w~90° (75°-105° bin) and θ_w~30° (15°-45° bin), both sorted into the *5m/s*-horizontal-wind-speed-bins from *0* to *90m/s*. The curves are cut off at high wind speeds (>*90m/s*) to ensure enough (at least *300*) samples in each wind-speed-bin. Two variance modes now have distinct differences. First, for wind speeds less than about *60m/s*, although both groups of variances increase with wind speed, the variances at θ_w~90° (Figure 3a) increase at a relatively faster rate than the other (especially at altitudes≤*53km*). Second, as wind speed exceeds about *60m/s*, different processes may have started to control these variances. The variances at θ_w~30° continue to grow, but the variances at θ_w~90° are saturated.

Furthermore, we map the radiance variances associated with θ_w~90° and θ_w~30° modes in Figure 4a,b, where the UKMO wind field averaged over the 1994-1997 winters are overlapped. Interestingly, the variances at θ_w~90° are mostly found around the center of the vortex over Alaska, Canadian High Arctic, Greenland and northeastern Europe, whereas the variances at θ_w~30° are mainly located near the edge of the polar vortex.

4. Discussions

Some of the observed characteristics in MLS radiance variances can be explained by interactions of propagating gravity waves with the background winds. Because the wave vertical wavelength (λ_z) spectrum can be Doppler-shifted into/out of the MLS filter (λ_z>*10km*), the radiance variances could increase or decrease accordingly when the background wind is intensified or weakened. The simplest form to relate the vertical wavelength to the background wind is:

$$\lambda_z = 2\pi (c - U\cos\theta_p)/N \qquad (1)$$

where c is the wave horizontal phase speed, U is the horizontal background wind speed, θ_p is the angle between the wind and wave propagation direction, and N is buoyancy frequency. Obviously when the wave propagates in the opposite direction of the wind (i.e. θ_p=*180°*), the Doppler shifting effect is the largest. In this case, the wave front is nearly perpendicular to the wind direction. This suggests that the observed variances at θ_w~*90°* (Figure 2) might correspond to the waves propagating closely to the opposite direction of the wind. In other words, these waves propagate mostly westward with actual path dips and rises following the opposite wind direction. For waves propagating in the same direction of the wind (i.e. θ_p<<*90°*), their wave fronts are also nearly perpendicular to the wind direction. However, because such waves are Doppler shifted to the shorter λ_z, they likely fall outside the MLS filter and their contributions are expected to be very weak.

The waves related to the variances at θ_w~*30°* viewing angle are relatively less affected by the Doppler-shifting since the wave fronts are nearly parallel to the wind direction. Our study using the limb-scan data (which is not shown here) suggests they are likely propagating southward from inside to outside of the vortex because the limb-scan measurements have a asymmetric response function in the θ_k-dependence [*Wu and Jiang*, 2000]. However, without the additional information, both polar-ward or equator-ward propagations are possible.

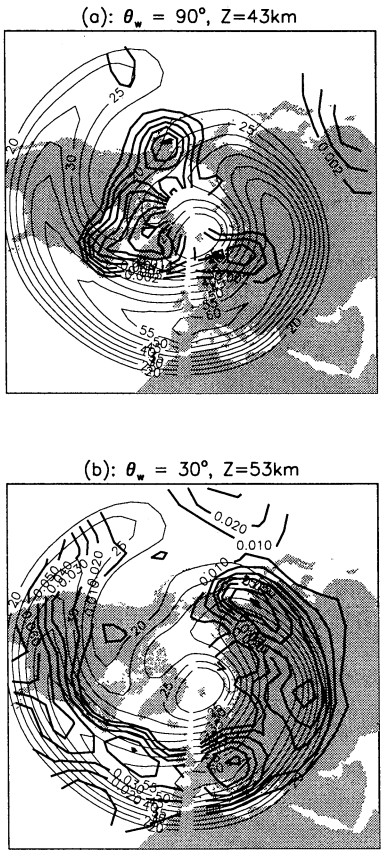

Figure 4. Maps for the radiance variances in the θ_w=*90°* viewing angle bin (a), and the θ_w=*30°* viewing angle bin (b). Thick contours are radiance variances, light contours are UKMO wind, both averaged over DJF of 1994-1997.

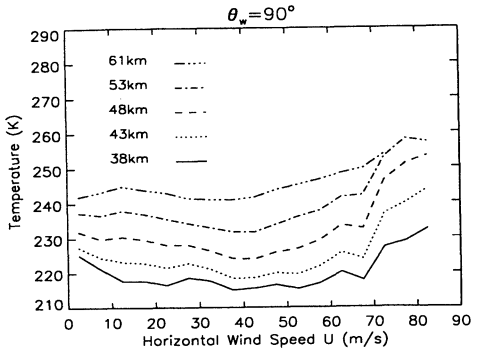

Figure 5. Mean air temperatures (1994-1997 DJF) sorted into different horizontal wind speeds near the θ_w=90° viewing angle region (around the center of Arctic polar vortex).

The fact that the θ_w~90° variance increases at a faster rate with wind speed than those at θ_w~30° in the background winds <60m/s (see Figure 3) may be explained as the result of wave propagation direction differences. Because the former propagates more toward the opposite direction of the wind, they are subject to larger Doppler shifting effect. However, the saturation of the θ_w~90° variance at wind speed >60m/s is not expected by the Doppler shifting, and one must seek other mechanisms to account for it. We further sort the mean air temperatures in the same way as the variances obtained in Figure 3. As wind speed exceeds ~60m/s, the air temperatures associated with those θ_w~90° variances increase by about 20°C (see Figure 5), whereas little temperature change is found for the temperatures associated with the θ_w~30° variances. Is the warmer air temperature coincident with the wave breaking and saturation? Wave breaking occurs when they become statically unstable if dense air is lifted by the waves to such a degree that it overlies less dense air somewhere in the wave-field. Recent Lidar observations conducted by *Duck et al.*, [1998] also reveal a wintertime warming of the upper stratosphere occurred in the winter polar vortex central area, which was suggested to be related to the breaking gravity waves. Their interpretation is that gravity wave breaking in the vortex jet might trigger turbulences and drags above the jet-stream maximum, producing a small inflow to center of the vortex. The ensuing masses pile-up then compress the underlying airmass, which warms the air adiabatically. However, the results presented in Figure 5 and Figure 3a seem to suggest that at least part of the warming could be directly related to a local heating source from wave breaking inside the vortex. Upon the wave breakdown, part of the potential energy E_p associated with gravity waves will be converted into kinetic energy E_k that modifies the local airflow, and part of the E_p will become thermal energy E_T, which can be estimated by

$$E_T = \frac{3}{2} nk\Delta T \qquad (2)$$

where n is the number of molecules per kilograms of air. Substituting in the Boltzmann constant $k=1.38\times10^{23} J\cdot K^{-1}$, and ΔT~20°C (estimated from Figure 5) for an ideal gas, one obtains that at *1 mb* pressure (i.e. altitude ~50km) the thermal energy released by the wave breaking is $\sim 6 J\cdot kg^{-1}$, which is close to the potential energy density ($\sim 10 J\cdot kg^{-1}$) estimated from both the lidar data by Whiteway et al. [1997], and the GPS occultation data by Tsuda et al. [2000].

Acknowledgments. The authors would like to thank Drs. E.R. Kursinski, J.R. Holton, B.R. Sutherland and J.W. Waters for valuable discussions. This research was conducted at the Jet Propulsion Laboratory, California Institute of Technology, under contract with the National Aeronautics and Space Administration. The research is supported by the NASA New Investigators Program of Earth Sciences, and UARS grant number NAFG-5-7090.

References

Alexander, M. J., Interpretations of observed climatological patterns in stratospheric gravity wave variance, *J. Geophys. Res., 103*, 8627-8640, 1998.

Duck, T.J., J. A. Whiteway, and A. I. Carswell, Lidar observations of gravity wave activity and Arctic stratospheric vortex core warming, *Geophys. Res. Lett., 25*, 2813-2816, 1998.

Fetzer, E.J., and J.C. Gille, Gravity wave variance in LIMS temperatures. Part I: Variability and comparison with background winds, *J. Atmos. Sci., 51*, 2461-2483, 1994.

McLandress, C., M.J. Alexander, and D.L. Wu, Microwave Limb Sounder observations of gravity waves in the stratosphere: A climatology and interpretation, *J. Geophys. Res, 105*, 11,947-11,967, 2000.

Preusse, P., B. Schaeler, J. Bacmeister, and D. Offermann, Evidence for gravity waves in CRISTA temperatures, *Adv. Space Res., 24*, 1601-1604, 1999.

Tsuda, T., M. Nishida, C. Rocken, R.H. Ware, A global morphology of gravity wave activity in the stratosphere revealed by the GPS occultation data (GPS/MET), *J. Geophys. Res, 105*, 7257-7273, 2000

Whiteway, J.A., T.J. Duck, D.P. Donovan, J.C. Bird, S.R. Pal, and Carswell, Measurements of gravity wave activity within and around the Arctic stratospheric vortex, *Geophys. Res. Lett., 24*, 1387-1390, 1997.

Wu, D.L., and J.H. Jiang, Mapping Atmospheric Gravity Wave Activity with Limb-Viewing Microwave Radiometer (UARS MLS), *Proceedings of IEEE 2000 International Geoscience and Remote Sensing Symposium*, 2000.

Wu, D.L., and J.W. Waters, Satellite observations of atmospheric variances: A possible indication of gravity waves, *Geophys. Res. Lett, 23*, 3631-3634, 1996a.

Wu, D.L., and J.W. Waters, Gravity-wave-scale temperature fluctuations seen by the UARS MLS, *Geophys. Res. Lett., 23*, 3289-3292, 1996b.

Wu, D.L., and J.W. Waters, Observations of Gravity Waves with the UARS Microwave Limb Sounder, *Gravity Wave Processes, NATOASI Series I: Global Environmental Change, 50*, 103-120, 1997.

Jonathan H. Jiang and Dong L. Wu, NASA Jet Propulsion Laboratory, California Institute of Technology, Mail-Stop: 183-701, 4800 Oak Grove Drive, Pasadena, California 91109-8099, U.S.A. (e-mail: jonathan@mls.jpl.nasa.gov or dwu@mls.jpl.nasa.gov)

(Received May 17, 2000; revised November 28, 2000; accepted November 29, 2000.)